Analysis of the Magneto-Mechanical Anisotropy of Steel Sheets in Electrical Applications

F. Martin[1], U. Aydin[1], A. Ruzibaev[1], Y. Ge[2], L. Daniel[3], L. Bernard[4], P. Rasilo[5], A. Benabou[6], and A. Belahcen[1]

[1]Department of Electrical Engineering and Automation, Aalto University, 02150 Espoo, Finland
[2]Department of Chemistry and Materials Science, Aalto University, 02150 Espoo, Finland
[3]GeePs, UMR CNRS 8507, CentraleSupélec, Univ. Paris-Sud, Univ. Paris-Saclay, Sorbonne Univ., 75006 Gif-sur-Yvette, France
[4]GRUCAD/EEL/CTC, Universidade Federal de Santa Catarina, Florianpolis 88040-900, Brazil
[5]Unit of Electrical Engineering, Tampere University, 33720 Tampere, Finland
[6]L2EP, Université Lille 1, 59650 Villeneuve d' Ascq, France

We investigate the effect of magneto-mechanical and magnetocrystalline anisotropies in a test application by coupling a multiscale magneto-mechanical model with a finite element method. This first application is composed of a cylindrical conductor surrounded by a ring composed of a non-oriented $FeSi_{3\%}$ steel sheet which contains 396 representative grain orientations. Such an application can reveal the anisotropy due to the texture of the material by inducing a rotational flux density within the ring. Moreover, the effect of the texture and the magneto-mechanical characteristic of the steel sheets is analyzed in an axially laminated synchronous reluctance machine. The effect of stress strongly emphasizes the anisotropic behavior of NO steel sheets.

Index Terms— **Finite element method, magnetic material, magneto-crystalline anisotropy, magnetostriction, multiscale model.**

I. Introduction

NON-ORIENTED steel sheets can enhance the performance of electrical applications by amplifying the magnetic flux in the active regions. In order to reduce their anisotropic behavior, these electrical steel sheets are composed of many grains with various orientations [1]. However, the magnetic anisotropy of non-oriented steel sheets still persists and the mechanical stress due to shrink-fitting and centrifugal forces amplifies the anisotropic behavior of the sheets. Hence, evaluating the performance of an electrical application requires an accurate magneto-mechanical model of the steel sheets.

Magneto-mechanical models can be derived from thermodynamic laws whose parameters are determined from the symmetry of the material and identified from magneto-mechanical measurements [2]–[4]. Other approaches rely on the definition of an equivalent isotropic crystal to describe the magneto-mechanical behavior of steel sheets with a simplified multiscale model [5]. Although these material models can be implemented into the finite element method [6], the magnetic anisotropy due to the texture is neglected. In [7], the anisotropic material is represented by an equivalent homogeneous anisotropic single crystal. Although such material representation can be embedded into the finite element method, the effect of the material texture on the application performances cannot be correctly assessed [7]. The discrepancy observed by the authors may be due to the omission of some terms with higher order in the equivalent single-crystal energy for representing a significant number of grain orientations. Finally, the multiscale model developed in [1] can account for the polycrystal texture so that the magneto-mechanical response is influenced by the magnetic field, the mechanical stress, and the magneto-crystalline anisotropy. However, such a model still remains computationally intensive so that it has not been implemented into the finite element method.

In this article, we propose implementing the magneto-mechanical multiscale model developed in [1] without its localization step into a finite element method. First, the multiscale model and the magneto-mechanical finite element formulation are developed in order to reduce the computational effort involved by the material model. Then, the technique to efficiently incorporate the multiscale model into the finite element method is described. Furthermore, two applications are presented: one allows analyzing the texture anisotropy with a reduced number of elements, and the other analyzes the effect of anisotropy in an axially laminated synchronous reluctance machine. Finally, it is shown that the effect of stress due to shrink fitting and centrifugal forces strongly emphasizes the anisotropic behavior of NO steel sheets.

II. Finite Element Method With Multiscale Model

A. Magneto-Mechanical Multiscale Model

The multiscale model describes the heterogeneity of the polycrystalline aggregate by introducing a set of grain orientations. A set of grains with the same orientation can be represented by a single crystal with a specific orientation and volume fraction. The single crystal energy W_c can be

Manuscript received August 19, 2019; accepted September 30, 2019. Date of current version January 20, 2020. Corresponding author: F. Martin (e-mail: floran.martin@aalto.fi).

Color versions of one or more of the figures in this article are available online at http://ieeexplore.ieee.org.

Digital Object Identifier 10.1109/TMAG.2019.2945181

decomposed into the magneto-static energy W_h, the magneto-mechanical energy W_σ, and the magnetocrystalline anisotropy energy W_{an} as

$$W_c = W_h + W_\sigma + W_{\text{an}}. \tag{1}$$

The magneto-static energy depends on the magnetic field $\vec{h}$ as

$$W_h = -\mu_0 M_s \vec{h} \cdot \vec{\gamma}_c \tag{2}$$

where μ_0 is the vacuum permeability, M_s is the saturation magnetization, and $\vec{\gamma}_c$ is the domain magnetization direction.

The magneto-mechanical energy is influenced by the applied stress $\mathfrak{o}$ as

$$W_\sigma = -\mathfrak{o} : \mathfrak{e}_c^\mu \tag{3}$$

where the magnetostriction tensor $\mathfrak{e}_c^\mu$ depends on the saturation magnetostriction constants λ_{100} and λ_{111}. It is assumed isochoric and is expressed, for cubic crystals, by

$$\mathfrak{e}_c^\mu = \begin{bmatrix} \lambda_{100}\left[{\gamma_{c_1}}^2 - \frac{1}{3}\right] & \lambda_{111}\gamma_{c_1}\gamma_{c_2} & \lambda_{111}\gamma_{c_1}\gamma_{c_3} \\ \lambda_{111}\gamma_{c_2}\gamma_{c_1} & \lambda_{100}\left[{\gamma_{c_2}}^2 - \frac{1}{3}\right] & \lambda_{111}\gamma_{c_2}\gamma_{c_3} \\ \lambda_{111}\gamma_{c_3}\gamma_{c_1} & \lambda_{111}\gamma_{c_3}\gamma_{c_2} & \lambda_{100}\left[{\gamma_{c_3}}^2 - \frac{1}{3}\right] \end{bmatrix}. \tag{4}$$

The magnetocrystalline anisotropy energy which depends on the magnetocrystalline anisotropy constants K_1 and K_2, is given, for cubic crystals, by

$$W_{an} = K_1\left({\gamma_{c_1}}^2{\gamma_{c_2}}^2 + {\gamma_{c_2}}^2{\gamma_{c_3}}^2 + {\gamma_{c_3}}^2{\gamma_{c_1}}^2\right) + K_2{\gamma_{c_1}}^2{\gamma_{c_2}}^2{\gamma_{c_3}}^2. \tag{5}$$

The directions $\vec{\gamma}_c$ of the six magnetic domains can be determined by minimizing the single crystal energy. The volume fraction f_c of each domain can be evaluated by maximizing the statistical entropy with a Boltzmann distribution such as

$$f_c = \frac{\exp(-A_s W_c)}{\sum_{d=1}^{6} \exp(-A_s W_d)} \tag{6}$$

where A_s depends on the initial susceptibility χ_0 of the material $A_s = 3\chi_0/(\mu_0 M_s^2)$.

The magnetization and the magnetostriction in a grain are determined by

$$\vec{m}_g = M_s \sum_{c=1}^{6} f_c \vec{\gamma}_c, \quad \mathfrak{e}_g^\mu = \sum_{c=1}^{6} f_c \mathfrak{e}_c^\mu. \tag{7}$$

The magneto-mechanical response of the material at the macroscopic scale is determined by considering the contribution of every grain with their volume fraction p_g such as

$$\vec{m} = \sum_{g=1}^{N_g} p_g \vec{m}_g, \quad \mathfrak{e}^\mu = \sum_{g=1}^{N_g} p_g \mathfrak{e}_g^\mu. \tag{8}$$

B. Finite Element Method

The elastic weak formulation is expressed in terms of displacement. It depends on the compliance tensor $\mathbb{C}$, the body force $\vec{f}$, the surface stress vector $\vec{t}$, and eventually on the thermal dilatation $\mathfrak{a}\Delta T$. The formulation is given by integration over the volume geometry Ω by

$$\int_\Omega \frac{1}{2}\mathbb{C} : (\mathfrak{e} - \mathfrak{e}^\mu - \mathfrak{a}\Delta T) : \mathfrak{e}' dV = \int_\Omega \vec{f} \cdot \vec{v} dV + \int_{\partial\Omega} \vec{t} \cdot \vec{v} dA \tag{9}$$

where the total strain $\mathfrak{e}$ is derived from the displacement vector $\vec{u}$. It is given by

$$\mathfrak{e} = \frac{1}{2}[\nabla\vec{u} + (\nabla\vec{u})^{\mathrm{T}}]. \tag{10}$$

The test function $\vec{v}$ for the displacement vector leads to $\mathfrak{e}'$.

The non-linear magnetostatic problem is formulated with the mixed formulation $\vec{h} - \vec{a}$ [8], [9] in order to avoid the numerical inversion of the multiscale model. In every element, the magnetic field $\vec{h}$ is supported by Whitney elements [10], whereas the magnetic vector potential $\vec{a}$, which corresponds to a Lagrange multiplier for conserving the flux density, is modeled with Lagrangian elements. This formulation is given for a Newton–Raphson iterative technique by

$$\begin{cases} \int_\Omega \mu_0 \left[\mathbb{I} + \frac{\partial\vec{m}}{\partial\vec{h}}(\vec{h}^k)\right]\delta\vec{h} \cdot \delta\vec{h}' - \delta\vec{a} \cdot [\nabla \times \delta\vec{h}']dV \\ \quad = \int_\Omega \vec{a}^k \cdot [\nabla \times \delta\vec{h}'] - \mu_0[\vec{h}^k + \vec{m}(\vec{h}^k)] \cdot \delta\vec{h}' dV \\ \int_\Omega [\nabla \times \delta\vec{h}] \cdot \delta\vec{a}' dV = \int_\Omega \vec{j} \cdot \delta\vec{a}' - \nabla \times \delta\vec{h}^k \cdot \delta\vec{a}' dV \end{cases} \tag{11}$$

where $\vec{j}$ is the current density in the conductors and $\mathbb{I}$ is the second-order identity tensor. Both the magnetization $\vec{m}$ and the incremental susceptibility tensor $\partial\vec{m}/\partial\vec{h}$ are evaluated with the multiscale model at the magnetic field $\vec{h}^k$ computed at the previous iteration while considering the mechanical stress. After solving the finite element weak formulation, the updated field and magnetic vector potential are computed by

$$\vec{h}^{k+1} = \vec{h}^k + \delta\vec{h}, \quad \vec{a}^{k+1} = \vec{a}^k + \delta\vec{a}. \tag{12}$$

III. Results and Discussion

First, some guidelines are given for implementing the multiscale model into the finite element method. Then, the method is applied to two applications for the case of 2-D plane strain finite element analysis of a test application and an axially laminated synchronous reluctance machine.

In order to investigate the magnetic anisotropy due to the texture of NO steel sheets, we consider either an ideal isotropic texture or a realistic texture. The M400-50A realistic texture consists of 396 unique grain orientations [Fig. 1(a)] which are measured from electron backscatter diffraction (EBSD) measurements. Their corresponding grain volume fractions are estimated from the orientation distribution function [Fig. 1(b)], which are evaluated from X-ray analysis with cobalt anode on four different pole figures. The ideal texture [Fig. 1(c)] consists of 546 grain orientations with the same volume fraction. In both cases, the physical parameters correspond to the material constants of iron-based alloy doped with 3% silicon. They are reported in [11].

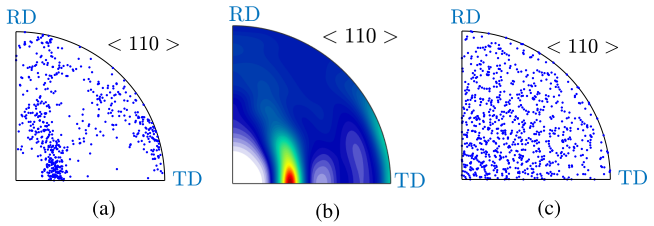

Fig. 1. Microstructure properties. Representations of the ⟨110⟩ pole figure of (a) and (b) NO material and (c) ideal isotropic texture.

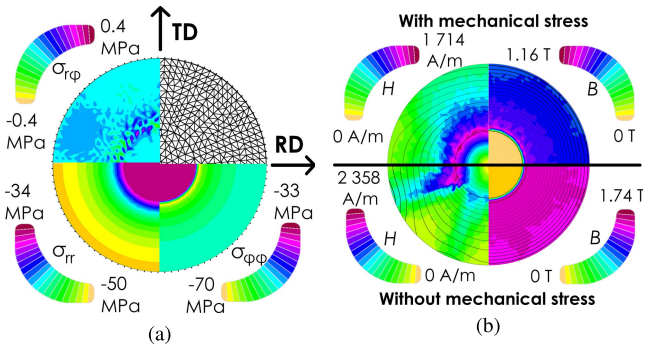

Fig. 2. Magneto-mechanical distribution in the test application. (a) Mesh and stress. (b) Effect of stress.

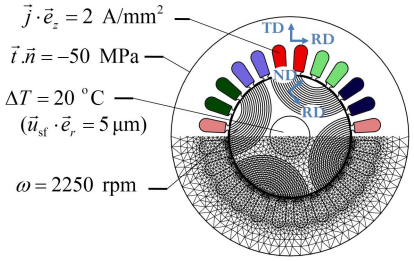

Fig. 3. Machine model and mesh. The full machine is modeled whereas only half of the mesh is presented. The lamination coordinate system is given with RD for RD, TD for TD, and ND for normal direction.

A. Implementation Technique

In order to efficiently implement the multiscale model into the finite element method, the domain orientations are determined with a Newton method which is initialized at the easy direction of the single crystal of each grain. For each new magneto-mechanical loading, the previous minima of the energy are employed as an initial guess of the Newton method. The Newton method is implemented by employing the *AVX 2* instructions of Intel processors. Hence, this set of assembler instructions can considerably speed up the determination of the domain orientations by avoiding unnecessary communication overload between the RAM memory and the processor registers. Furthermore, the magneto-mechanical response of each grain is computed in parallel with the *OpenMP* instructions by employing the reduction method for evaluating the macroscopic quantities (8). Finally, the multiscale model is embedded in a dynamic link library which is called by *FreeFEM* [12] in order to evaluate the constitutive law at each integration point of every element containing NO steel sheets.

The domain orientations of every grain in each integration point are kept in memory in order to efficiently determine the domain orientation matching with another magneto-mechanical loading. In the applications, 12 steps are employed to track these minima until the requested magneto-mechanical loading.

B. Test Application: Cylindrical Conductor With Magnetic Ring

The test application is composed of a cylindrical conductor surrounded by a ring composed of the steel sheet. The conductor carries a current density of 0.3 A/mm^2 and the external surface of the steel sheet is under a radial compression of 50 MPa. The mesh contains 1763 elements and 932 vertices. The $FeSi_{3\%}$ nonoriented steel sheet is modeled with the described multiscale model which accounts for 396 grain orientations [Fig. 1(a) and (b)]. This material model is incorporated into the described finite element method to model a 2-D test application.

In Fig. 2(a), the stress distribution is presented. In the steel sheet, it mainly consists of a compressive radial stress σ_{rr} and a compressive circumferential stress $\sigma_{\phi\phi}$. Such stress distribution is expected since the surface compression, imposed as a boundary condition, tends to compress both the radial and the circumferential directions in the cylindrical geometry. In Fig. 2(b), the bi-compressive stress state tends to decrease the magnetic flux density and field which become smaller near the external surface. Besides, the texture and stress also induce a magneto-mechanical anisotropy. In our material, the rolling direction (RD) is more sensitive to the stress than the transverse direction (TD). Once the stress is released, the anisotropy due to the texture of the sheet can be clearly noticed on the field distribution where harder directions present higher field amplitude for the same flux density. Moreover, the field lines indicate the anisotropic behavior of the field direction due to the material texture.

C. Axially Laminated Synchronous Reluctance Machine

The axially laminated synchronous reluctance machine, already described in [13], contains a stator with distributed winding and a rotor composed of a stack of steel laminations with interlaminar insulation sheets. The machine model and its mesh are represented in Fig. 3 with its magneto-mechanical sources. The rotation of the rotor generates centrifugal body forces along the radial direction: $\vec{f} = \rho\omega^2 r\vec{e}_r$ where ω is the rotor speed and ρ is the density. The machine mesh contains 9378 triangular elements with 4726 nodes. Although some convergence issue can be observed while accounting for the magnetic anisotropy of the steel sheets [14], the preservation of the orthotropic symmetry of the steel sheets by the multiscale model did not cause any divergence problem so that it requires about four iterations maximum to reach a converged magneto-mechanical solution. Besides, the computational time amounts to only 276 seconds for the 12 current steps on a *i7-6700HQ* processor with 8 GB of RAM.

First, the case without stress is considered. The anisotropic effect due to the texture is relatively small on the norm of

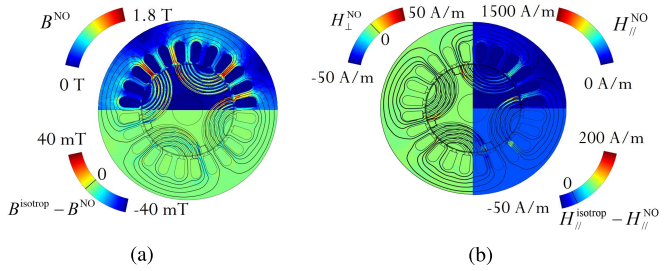

Fig. 4. Magnetic field and flux density distribution without considering mechanical stress. $H_{//}$ and $H_{\perp}$ are the magnetic field parallel and orthogonal to the flux density, respectively. The superscripts *NO* and *isotrop* refer to the texture measured in M400-50A and the ideal isotropic texture, respectively. (a) Flux density. (b) Magnetic field.

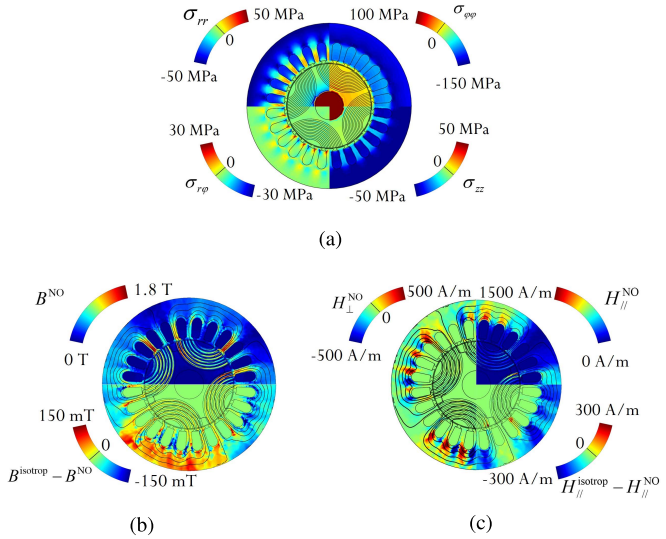

Fig. 5. Mechanical stress, magnetic field, and flux density distribution with the impact of mechanical stress. The orthogonal component of the magnetic field clearly points the area around the slots where the rotational effect occurs. (a) Mechanical stress. (b) Flux density. (c) Magnetic field.

the flux density and the magnetic field components [Fig. 4(a) and (b)] where most of the variations due to the texture are localized in the teeth and the rotor lamination.

Then, we investigate the effect of mechanical stress on the anisotropic behavior of NO steel sheets (Fig. 5). In Fig. 5(a), the stator yoke is under biaxial compression due to the shrink-fitting from the frame whereas the stator teeth experience a biaxial state with shear in the teeth corner. The rotor mainly withstands a radial compressive stress due to the shaft shrink-fitting. In Fig. 5(b), the effect of stress clearly affects the amplitude of the flux density. The isotropic assumption leads to an underestimation and an overestimation of the flux density amplitude by 15% in the teeth and 20% in the yoke, respectively. Moreover, the orthogonal component of the field clearly depicts the area around the slots where the rotational effect occurs [Fig. 5(c)]. Although such an effect was not revealed in the case without stress, it is emphasized by the biaxial compressive stress which tends to increase the amplitude of the magnetic field. The orthogonal component of the field can reach one-third of the parallel component which indicates a strong anisotropic behavior. Finally, the isotropic texture tends to underestimate the parallel component of the field by about 30% in the stator yoke.

IV. Conclusion

In this article, we proposed an efficient method to incorporate the multiscale magneto-mechanical model into the finite element method. The computational burden due to the determination of the magneto-mechanical properties of each grain at every integration point was significantly reduced by employing the *AVX 2* instructions and the parallelization of the calculation with one core per grain. The first application, which consists of a cylindrical conductor surrounded by a ring of NO steel sheets, can reveal the anisotropy due to the texture. Furthermore, the effect of texture anisotropy is demonstrated for an axially laminated synchronous reluctance machine. In this case, the mechanical stress tends to emphasize the difference in the magnetic quantities due to the material texture. Moreover, the isotropic texture can lead to underestimate the flux density in the stator teeth. In the future, the effect of the texture will be investigated in terms of losses, torque ripple, and flux linkage.

References

[1] L. Daniel, O. Hubert, N. Buiron, and R. Billardon, "Reversible magneto-elastic behavior: A multiscale approach," *J. Mech. Phys. Solids*, vol. 56, no. 3, pp. 1018–1042, Mar. 2008.

[2] C. Miehe, B. Kiefer, and D. Rosato, "An incremental variational formulation of dissipative magnetostriction at the macroscopic continuum level," *Int. J. Solids Struct.*, vol. 48, no. 13, pp. 1846–1866, Jun. 2011.

[3] P. Rasilo *et al.*, "Modeling of hysteresis losses in ferromagnetic laminations under mechanical stress," *IEEE Trans. Magn.*, vol. 52, no. 3, Mar. 2016, Art. no. 7300204.

[4] B. Nedjar, "A coupled BEM-FEM method for finite strain magneto-elastic boundary-value problems," *Comput. Mech.*, vol. 59, no. 5, pp. 795–807, May 2017.

[5] L. Daniel, O. Hubert, and M. Rekik, "A simplified 3-D constitutive law for magnetomechanical behavior," *IEEE Trans. Magn.*, vol. 51, no. 3, Mar. 2015, Art. no. 7300704.

[6] L. Bernard and L. Daniel, "Effect of stress on magnetic hysteresis losses in a switched reluctance motor: Application to stator and rotor shrink fitting," *IEEE Trans. Magn.*, vol. 51, no. 9, pp. 1–13, Sep. 2015.

[7] D. Vanoost *et al.*, "Embedding a magnetoelastic material model in a coupled magnetomechanical finite-element solver," *IEEE Trans. Magn.*, vol. 51, no. 11, pp. 1–4, Nov. 2015.

[8] A. Bossavit, "Mixed finite elements and the complex of whitney forms," in *The Mathematics of Finite Elements and Applications VI*, J. Whiteman, Ed. London, U.K.: Academic, 1988, pp. 137–144.

[9] P. Dular, J.-F. Remacle, F. Henrotte, A. Genon, and W. Legros, "Magnetostatic and magnetodynamic mixed formulations compared with conventional formulations," *IEEE Trans. Magn.*, vol. 33, no. 2, pp. 1302–1305, Mar. 1997.

[10] H. Whitney, *Geometric Integration Theory*. Princeton, NJ, USA: Princeton Univ. Press, 1957.

[11] L. Daniel, M. Rekik, and O. Hubert, "A multiscale model for magneto-elastic behaviour including hysteresis effects," *Arch. Appl. Mech.*, vol. 84, nos. 9–11, pp. 1307–1323, Oct. 2014.

[12] F. Hecht, "New development in freefem++," *J. Numer. Math.*, vol. 20, nos. 3–4, pp. 251–265, Dec. 2012.

[13] F. Martin *et al.*, "Magneto-mechanical analysis of an axially laminated synchronous reluctance machine," in *Proc. ICEM*, Sep. 2016, pp. 1861–1867.

[14] F. Martin, D. Singh, P. Rasilo, A. Belahcen, and A. Arkkio, "Model of magnetic anisotropy of non-oriented steel sheets for finite-element method," *IEEE Trans. Magn.*, vol. 52, no. 3, Mar. 2016, Art. no. 7002704.